REALIZABLE DYNAMIC LES SUBGRID-SCALE MODELING

Stefan Heinz
Department of Mathematics
University of Wyoming
1000 E. Univ. Ave., Laramie WY 82071, USA
heinz@uwyo.edu

Harish Gopalan
Department of Mechanical Engineering
NUS Keppel Corporate Research Lab
Engineering Drive 1, Singapore 117575
harish.gopalan@gmail.com

Ehsan Kazemi Foroushani
Department of Mathematics
University of Wyoming
1000 E. Univ. Ave., Laramie WY 82071, USA
ehsan_kf61@yahoo.com

Michael K. Stoellinger
Mechanical Engineering Department
University of Wyoming
1000 E. Univ. Ave., Laramie WY 82071, USA
mstoell@uwyo.edu

Reza Mokhtarpoor
Department of Mathematics
University of Wyoming
1000 E. Univ. Ave., Laramie WY 82071, USA
rmokhtar@uwyo.edu

Ponnampalam Balakumar
Flow Physics and Control Branch
NASA Langley Research Center
Hampton, VA 23681, USA
ponnampalam.balakumar-1@nasa.gov

ABSTRACT

It was shown recently that the use of stochastic analysis enables a theoretically well based systematic derivation of a realizable linear dynamic model (LDM) and a realizable nonlinear dynamic model (NDM). *A-priori* and *a-posteriori* analyses of turbulent channel flow and the turbulent Ekman layer are used to study the characteristic properties of these dynamic models. The LDM and NDM are compared with other dynamic models: the non-stabilized and stabilized dynamic Smagorinsky model (DSM), which is used in many applications of LES, and Wang-Bergstrom's dynamic model (WBDM), which represents an extension of the DSM. The DSM and WBDM do not represent realizable models because they are not derived as consequences of a realizable stochastic process. The comparisons reported here show that the LDM and NDM are based on a dynamic model formulation that avoids shortcomings of existing concepts. The LDM and NDM account for backscatter, and they are computationally stable without any modification. The LDM and NDM represent the instantaneous small scale structure of turbulence very well. Compared to the DSM and WBDM, respectively, the LDM and NDM are computationally more efficient.

INTRODUCTION

Large Eddy Simulation (LES) represents a very promising method to address many relevant engineering and environmental problems. The price for reducing the computational cost of direct numerical simulation (DNS) by the consideration of LES equations is a closure problem given by the appearance of the unknown deviatoric subgrid-scale (SGS) stress tensor τ_{ij}^d in LES equations. The simple Smagorinsky model $\tau_{ij}^d = -2\nu_t \widetilde{S}_{ij}$ is often used as a model for the deviatoric SGS stress, where incompressible flow is considered for simplicity. Here, $\widetilde{S}_{ij}$ refers to the filtered rate-of-strain tensor and $\nu_t = C_S \Delta^2 |\widetilde{S}|$ is the SGS viscosity. This viscosity involves the Smagorinsky constant C_S, the filter width Δ, and the filtered characteristic strain rate $|\widetilde{S}| = (2\widetilde{S}_{ij}\,\widetilde{S}_{ji})^{1/2}$. The sum convention is used in this paper. The calculation of the SGS stress using the Smagorinsky model requires the setting of C_S. The simplest choice is a constant positive C_S value. However, there are two main problems associated with the use of a constant C_S. First, a constant C_S turned out to be inappropriate to accurately calculate, for example, laminar flows, transitional flows and near-wall regions. Second, the Smagorinsky model cannot account for backscatter of energy from the small scales to large scales, which requires negative C_S values.

Many dynamic LES methods were presented over the last two decades. Thus, there is the question of which dynamic method should be preferred. The goal of this paper is to provide evidence that the dynamic SGS stress models proposed by Heinz (2008) have significant advantages compared to usually applied dynamic SGS stress models. The performance of dynamic SGS models obtained via stochastic analysis will be investigated here in terms of turbulent channel flow simulations and turbulent Ekman layer simulations (Heinz & Gopalan, 2012; Kazemi, 2014). Two other dynamic models will be applied for comparisons, the stabilized DSM, which is used in many applications of LES, and Wang-Bergstrom's dynamic model (WBDM) (Wang & Bergstrom, 2005), which represents an extension of the DSM. After a brief introduction of models, the performance of the new dynamic models will be highlighted in the following three sections. Conclusions will be presented finally.

REALIZABLE DYNAMIC LES SGS MODELS

The LES modeling approaches applied below are based on the incompressible Navier-Stokes equations for filtered velocities $\widetilde{u}_i$ ($i = 1, 3$),

$$\frac{\partial \widetilde{u}_i}{\partial x_i} = 0, \tag{1}$$

$$\frac{\widetilde{D}\widetilde{u}_i}{\widetilde{D}t} = -\frac{1}{\rho}\frac{\partial P}{\partial x_i} + 2\nu\frac{\partial \widetilde{S}_{ij}}{\partial x_j} - \frac{\partial \tau_{ij}^d}{\partial x_j} - 2\varepsilon_{3ji}\Omega_j\widetilde{u}_i. \tag{2}$$

Here, $\widetilde{D}/\widetilde{D}t = \partial/\partial t + \widetilde{u}_k\partial/\partial x_k$ denotes the filtered Lagrangian time derivative, ρ is the constant mass density, $P = \widetilde{p} + 2k/3$ is the modified filtered pressure that includes a contribution due to the SGS kinetic energy $k = \tau_{ii}/2$. $\widetilde{S}_{ij} = (\partial \widetilde{u}_i/\partial x_j + \partial \widetilde{u}_j/\partial x_i)/2$ is the filtered rate-of-strain tensor, ν is the constant kinematic viscosity, and τ_{ij}^d refers to the deviatoric part of SGS stress tensor τ_{ij}. The last term on the right-hand side of Eq. (2) reflects the Coriolis force effect, which is only involved in the Ekman layer simulations reported below. With respect to channel flow simulations, the wall normal direction is x_2 (y). With respect to Ekman layer simulations, the wall normal direction is x_3 (z). Ω_j refers to the rotation vector. The permutation symbol ε_{ijk} is $+1$ for cyclic values of ε_{ijk}, -1 for anti-cyclic values, and 0 if an index is repeated. The numerical grid with a filter width $\Delta = (\Delta_1\Delta_2\Delta_3)^{1/3}$ is used as LES filter.

Equation (2) is unclosed as long as the deviatoric SGS stress tensor τ_{ij}^d is not defined. We will apply the usual eddy-viscosity model for τ_{ij}^d,

$$\tau_{ij}^d = -2\nu_t\widetilde{S}_{ij} = -2C_S\Delta^2|\widetilde{S}|\widetilde{S}_{ij}. \tag{3}$$

The SGS viscosity ν_t is defined via the last expression. The LES models described in the following subsections differ by their different ways to define the model parameter C_S.

A dynamic method for calculating C_S offers many advantages. The model considered here is the dynamic model suggested by Germano (1992); Germano *et al.* (1991) combined with the modification of Lilly (1992), which forms the basis for many dynamic LES models,

$$C_S = -\frac{L_{ij}^d H_{ij}}{H_{mn}H_{mn}}. \tag{4}$$

Here, H_{ij} and the Leonard stress tensor L_{ij}, which enters Eq. (4) via its deviatoric part L_{ij}^d, are given by

$$H_{ij} = 2(\Delta^T)^2|\overline{\widetilde{S}}|\overline{\widetilde{S}}_{ij} - 2(\Delta)^2\overline{|\widetilde{S}|\widetilde{S}_{ij}}, \quad L_{ij} = \overline{\widetilde{u}_i\widetilde{u}_j} - \overline{\widetilde{u}}_i\overline{\widetilde{u}}_j. \tag{5}$$

The overbar refers to the test filter operation, and Δ^T is the test filter width. It is worth noting that both H_{ij} and L_{ij} are available in simulations. The combination of the SGS model (3) with (4) for C_S will be referred to below as original dynamic Smagorinsky (DSM) model.

Unfortunately, the original DSM usually cannot be applied in simulations. It leads to the appearance of large negative values of C_S, which imply computational instabilities. To stabilize the DSM, we will apply Eq. (4) averaged along cell faces,

$$C_S = -\frac{\langle L_{ij}^d H_{ij}\rangle}{\langle H_{mn}H_{mn}\rangle}, \tag{6}$$

where $\langle\ldots\rangle$ refers to a local averaging over cell faces. In addition, the total viscosity $\nu + \nu_t$ is clipped to zero whenever
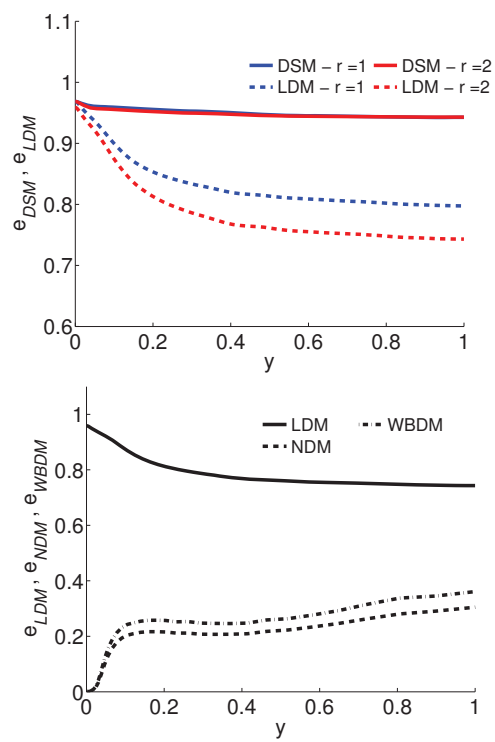
Figure 1. The standardized error $e = \left[|E|/|L^d|\right]^2$ of the DSM and LDM is shown in above for $r = \Delta^T/\Delta = 1$ and $r = 2$. Below, the LDM error is compared to the errors of the nonlinear NDM and WBDM for $r = 2$.

it is negative. The combination of the SGS model (3) with (6) for C_S will be referred to below as stabilized DSM.

As an alternative to the stabilized DSM, we also consider another dynamic LES model, which was derived on the basis of stochastic analysis Heinz (2008); Heinz & Gopalan (2012),

$$C_S = -\frac{L_{ij}^d M_{ji}}{M_{kl}M_{lk}}. \tag{7}$$

Here, L_{ij}^d is defined according to expressions (5), and the matrix M_{ij} is given by the expression

$$M_{ij} = 2(\Delta^T)^2|\overline{\widetilde{S}}|\overline{\widetilde{S}}_{ij}. \tag{8}$$

The combination of the SGS model (3) with (7) for C_S will be referred to below as realizable linear dynamic model (LDM). This model was used here without any averaging or clipping of the dynamic coefficient.

The essential difference between Eq. (7) and the two DSM models (4), (6) is that they are based on different assumptions for the deviatoric Leonard stress L_{ij}^d. Both DSM models assume $L_{ij}^d = -C_S H_{ij}$, whereas the LDM applies $L_{ij}^d = -C_S M_{ij}$. The expressions for C_S are implied by the corresponding L_{ij}^d assumptions Heinz (2008); Heinz & Gopalan (2012): by defining an quadratic error of L_{ij}^d assumptions (which is implied by any setting of C_S) and minimizing this error, one obtains Eqs. (7) and (4).

MODEL PERFORMANCE ANALYSES

A-priori channel flow analyses of the non-stabilized DSM, WBDM, LDM, and NDM were used to study the suitability of formulations of dynamic models. An analysis of model errors showed very limited support for the model assumption of the DSM approach. On the other hand, the
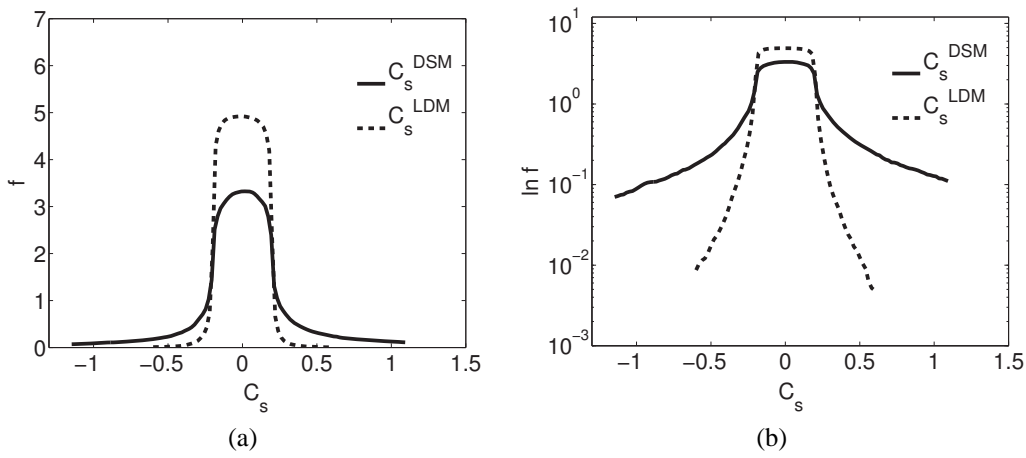
Figure 2. Comparison of the PDF of C_s obtained for the DSM and LDM: (a) PDF, (b) PDF logarithm, where $r = \Delta^T/\Delta = 2$. The PDFs were calculated for the horizontal slice at $y^+ = 40$.

model assumption used in the LDM has a much higher level of support: the correlation value $r_{LM} = 0.5$ obtained away from the near-wall region is 2.5 times higher than the corresponding value $r_{LH} = 0.2$ obtained for the DSM (see Fig. 1). An analysis of correlation coefficients also showed that the LDM provides consistently significantly higher correlations than the DSM. Regarding the corresponding comparison of nonlinear dynamic models it is shown that the NDM always provides slightly higher correlation values than the WBDM, which represents an extension of Germano's dynamic concept.

A-priori channel flow analyses of the non-stabilized DSM, WBDM, LDM, and NDM were also used to study the stability properties of dynamic models. Regarding the LDM it was shown that the stochastic modeling concept provides (without the use of any empirical clipping procedure) a natural clipping of dynamic constant values. The corresponding DSM feature is very different: the probability of very high positive or negative dynamic constant values can be by two orders of magnitude higher than the corresponding LDM probability for finding such dynamic constant values (see Fig. 2). The relatively high probability for very high negative dynamic constant values explains the DSM trend to become computationally unstable. The comparison of the NDM and WBDM shows that the structure of the PDFs of dynamic constants involved is very similar. Thus, the WBDM, which uses a dynamic model formulation in correspondence to the DSM, is computationally stable. However, several observations support the view that there is no need for the introduction of the third dynamic constant involved in the WBDM. It appears that this third dynamic constant corresponds to the consideration of an additional noise source in dynamic calculations. Backscatter studies show that the DSM overpredicts the DNS backscatter in the near-wall region, which promotes the development of computational instabilities, whereas the LDM backscatter is below the DNS backscatter. The nonlinear NDM and WBDM models provide a significant improvement compared to the LDM, but such that their backscatter is below the DNS backscatter. Thus, the NDM and WBDM are found to be computationally stable.

MODEL APPLICATIONS: CHANNEL FLOW

The realizable dynamic stress models were applied to turbulent channel flow in the following way. The domain

size $(L_x * L_y * L_z)$ is taken to be $(2\pi * 2 * \pi)$ according to the DNS of Moser et al. Moser *et al.* (1999). All simulations were performed for a friction Reynolds number $Re_\tau = u_\tau \delta/\nu = 395$. Here, $u_\tau = \sqrt{\tau_w/\rho}$ is the friction velocity, τ_w refers to the wall shear stress, and δ is the half channel width. This Reynolds number was chosen to enable efficient DNS of a flow that is not significantly affected by Reynolds number effects.

DNS and LES were performed by using the Open-FOAM CFD Toolbox (2009). The dynamic LES models have been implemented inside the OpenFOAM CFD Toolbox. The calculations have been performed by using a finite-volume based method. The convection term in the momentum equation was discretized using a second-order central difference scheme. The pressure gradient that drives the flow in the channel has been adjusted dynamically to maintain a constant mass flow rate. The PISO algorithm was used for the pressure-velocity coupling Issa (1986). The resulting algebraic equation for all the flow variables except pressure has been solved iteratively using a preconditioned bi conjugate gradient method with a diagonally incomplete LU preconditioning at each time step. The Poisson equation for the pressure was solved using an algebraic multi-grid (AMG) solver. When the scaled residual became less than 10^{-6}, the algebraic equation was considered to be converged. Time marching was performed using a second-order backward difference scheme. The time step was modified dynamically to ensure a constant CFL number of 0.5. Periodic boundary conditions have been employed along the streamwise and spanwise direction for all the flow variables. Along the wall normal direction, a no slip boundary condition was employed for the velocity and a zero gradient boundary condition has been used for the pressure term. A uniformly distributed grid was used along the streamwise and spanwise directions while the grid was refined in the wall normal direction using a hyperbolic tangent function. The DNS were performed on a grid size of $384 * 256 * 256$. A much higher grid resolution was used compared to the simulations of Moser et al. Moser *et al.* (1999) ($256 * 193 * 192$) because the current study uses a lower-order finite difference scheme while the simulations of Moser et al. used a spectral code. Based on the recommendation of Gullbrand and Chow Gullbrand & Chow (2003), the LES were performed on a grid size of $81 * 64 * 81$. This grid size was suggested by Gullbrand and Chow Gullbrand & Chow (2003) to minimize the ef-

3
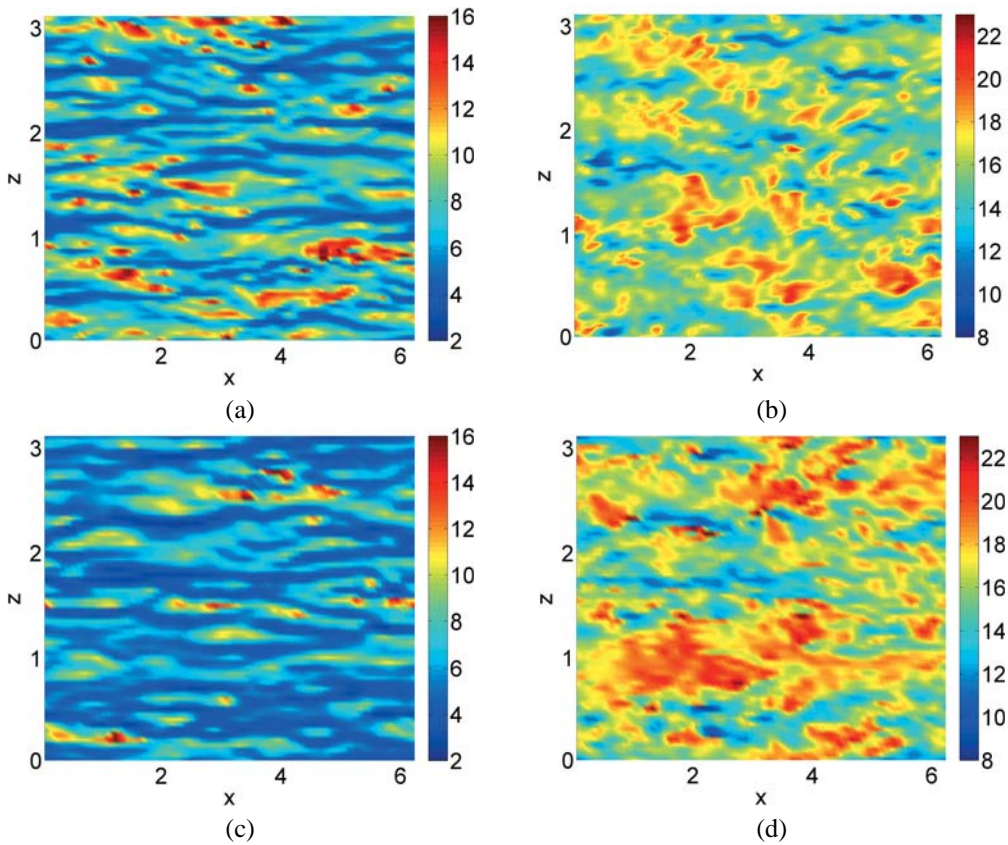
Figure 3. Instantaneous streamwise velocity contours at $y^+ = 5$ (left-hand side pictures) and $y^+ = 50$ (right-hand side pictures) obtained for the LDM (upper row) and DSM (lower row).

fect of numerical errors arising from second-order schemes. The numerical grid with a filter width $\Delta = \left(\Delta_x \Delta_y \Delta_z\right)^{1/3}$ was used as LES filter.

A-posteriori analyses of the stabilized DSM, WBDM, LDM, and NDM were used to study the accuracy of these dynamic methods. All the four dynamic models considered imply almost the same mean velocities and resolved Reynolds stresses. Differences are found with regard to instantaneous streamwise velocities. Due to the averaging and clipping involved, the DSM simulates turbulence structures that are smeared out and merged to large-scale structures, this means the small-scale structure of turbulence is not well represented (see Fig. 3). The LDM was shown to represent a better choice than the DSM. The LDM involves backscatter which enables an accurate representation of small-scale turbulence, and it is capable of correctly representing the typical streaky structures seen in the near-wall region of wall-bounded flows. Both the NDM and WBDM were found to provide predictions of instantaneous streamwise velocities that correspond to the LDM predictions.

A-posteriori analyses of the stabilized DSM, WBDM, LDM, and NDM were also used to study the cost of these dynamic methods. The computational cost of all the dynamic models considered scale with the number of grid points N in the same way. The relative cost ratio of dynamic models, which is independent of N, is given by $a = (1.000, 1.043, 1.068, 1.101)$ for the LDM, DSM, NDM, and WBDM, respectively. This result was obtained for N ranging from 0.3 to 10.7 million grid points.

MODEL APPLICATIONS: EKMAN LAYER

The equations considered were made nondimensional by using a characteristic velocity and length scale. With respect to the Ekman layer we consider the geostrophic wind velocity U_g and the Ekman layer depth $\delta_E = (2\nu/f)^{1/2}$, where f refers to the Coriolis parameter. By using these scaling variables we find the Ekman layer to be characterized by the nondimensional Reynolds number $Re = U_g \delta_E / \nu$. The Reynolds number determines the Rossby number $Ro = U_g/(f\delta_E)$ by the relation $Re = 2Ro$. Given the computational requirements for performing DNS we considered a DNS at $Re = 400$. For this Re, the computational DNS cost are still affordable. At the same time, the turbulence is sufficiently developed such that turbulence models can be tested: see Coleman *et al.* (1990), Marlatt (1994), and Shingai & Kawamura (2002). DNS was performed for a $(2\delta)^3$ domain on a 192^3 grid, where $\delta = u_*/f$. The LES results shown below where obtained for the same domain on a 96^3 grid.

The simulation were performed by using the Open-FOAM CFD Toolbox (2009), an unstructured finite-volume solver. The PISO algorithm was used for the pressure-velocity coupling in the Ekman layer simulations. The resulting algebraic equation for all the flow variables except pressure has been solved iteratively using a preconditioned bi conjugate gradient method with a diagonally incomplete LU preconditioning at each time step. The convection term in the momentum equation was discretized using a second-order central difference scheme. The geostrophic wind is maintained through the adjustment of the driving pressure gradient in the momentum equation by the rela-
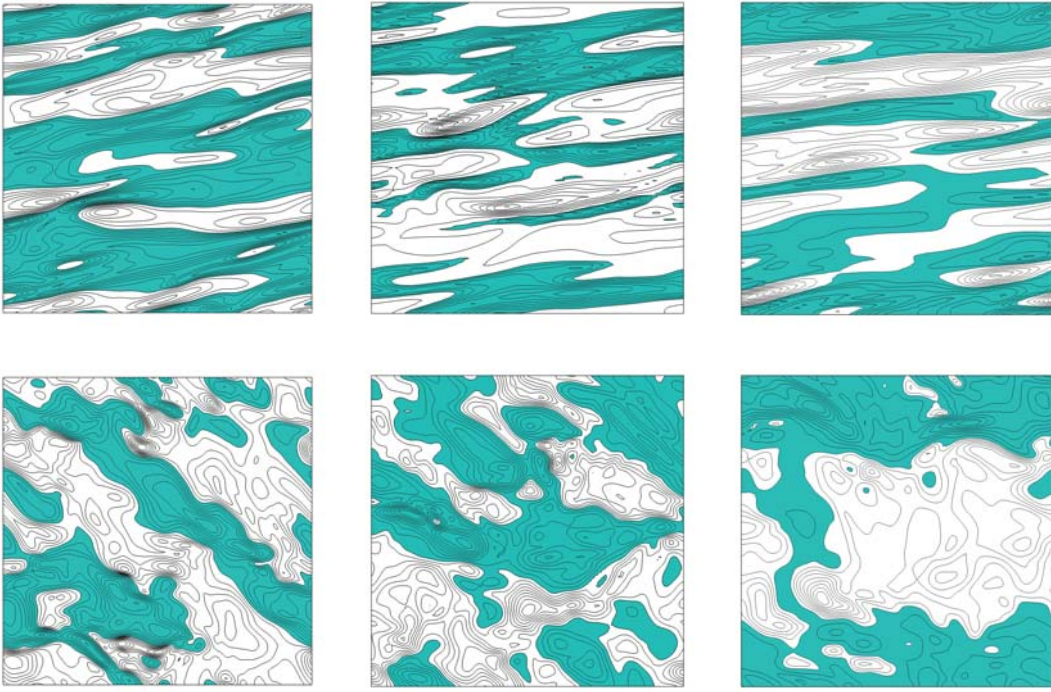
Figure 4. Instantaneous velocity fluctuations u'/u_* at $z^+ = 2.6$ (first row) and $z^+ = 87.6$ (second row): negative regions are colored. From left to right: DNS, LDM, and stabilized DSM.

tion $2\mathbf{\Omega} \times (U_g, 0, 0) = -\nabla p/\rho$. Here, $\mathbf{\Omega} = f\mathbf{k}/2$ refers to the rotation vector, where the unit vector in z direction is denoted by $\mathbf{k}$. In the case of LES, the Coriolis force and SGS viscosity are treated explicitly. The Poisson equation for the pressure was solved using an algebraic multigrid (AMG) solver. When the scaled residual became less than 10^{-7}, the algebraic equation was considered to be converged. Time marching was performed using a second-order Cranck-Nicolson scheme. Periodic boundary conditions have been employed along the streamwise and spanwise directions for all the flow variables. The non-slip condition is used on the bottom surface. At the top boundary, a slip-wall condition was specified for the velocity and zero gradient conditions for all other variables.

With respect to the mean flow it turned out that the dynamic models considered perform very well without revealing significant differences (Kazemi, 2014). Contours of the instantaneous velocity fluctuations u' in horizontal planes $z^+ = (2.6, 87.6)$ are shown in Fig. 4 at $tf = 2.3$. The contour interval is $\Delta = 0.15$. With respect to u' fluctuations at $z^+ = 2.6$, we see in DNS the typical long elongated structures close to a wall (Heinz & Gopalan, 2012). These streaks are very long, they continue throughout the whole domain. In contrast to channel flow we see a tilting of these structures, which is implied by the Coriolis force. The LDM is capable of producing approximately the same streaky structures seen in DNS. The stabilized DSM features are relatively similar with the exception that the fine scale structure is not so well resolved as given by the LDM (we observe larger areas of positive and negative velocity fluctuations). With respect to instantaneous velocity structures away from the wall at $z^+ = 87.6$, the DNS features differ from those seen at $z^+ = 2.6$ by two facts. First, the tilting is stronger and in the opposite direction. Second, we observe larger structures. The latter observation is a typ-

ical feature for turbulence away from the wall (the turbulent eddies increase with a growing wall distance), which is also seen in channel flow simulations (Heinz & Gopalan, 2012). Again, the LDM produces the same features as seen in DNS. With respect to the stabilized DSM, there are clear differences to DNS. First, there is no evidence for a tilting of instantaneous structures. Second, areas of positive and negative velocity fluctuations are much larger, this means the fine scale structure of turbulence is incorrectly represented.

SUMMARY

The comparisons reported here support the view that the LDM and NDM are based on a concept that is more appropriate than the concept used for obtaining the DSM and WBDM. An analysis of model errors shows very limited support for the model assumption of the DSM approach. On the other hand, the model assumption used in the LDM has a much higher level of support: the correlation value obtained away from the near-wall region is 2.5 times higher than the corresponding value obtained for the DSM. Regarding the LDM it was shown that the stochastic modeling concept provides (without the use of empirical clipping procedures) a natural clipping of dynamic constant values. The DSM feature is different: the probability of very high positive or negative dynamic constant values can be by two orders of magnitude higher than the corresponding LDM probability for finding such dynamic constant values. The relatively high probability for very high negative dynamic constant values explains the DSM trend to become computationally unstable. The LDM and NDM account for backscatter, and they are computationally stable without any modification. Compared to the DSM and WBDM, respectively, the LDM and NDM are computationally more efficient.

5

With respect to channel flow and Ekman layer applications, the analysis of LDM model features shows that the LDM is much more effective than the stabilized DSM with respect to the reduction of the range of negative C_S values. The LDM produces a mean velocity and stresses that agree well with DNS data. It produces instantaneous velocity fields that show the same fine scale turbulence structures close and away from the wall as seen in DNS. The effect of grid variations correctly shows that a gradual grid coarsening leads to a gradual reduction of turbulent stresses. On the other hand, the stabilized DSM predicts mean fields comparably well as the LDM. However, the analysis of instantaneous velocity fields reveals significant disadvantages: the stabilized DSM performance depends on the wall distance. Close to the wall, the stabilized DSM produces acceptable turbulence structures that agree, basically, with DNS. Away from the wall, the stabilized DSM suffers from shortcomings described at the end of the preceding section.

Overall, the following fact is surprising: the use of a dynamic LES method represents a mean for correctly simulating large-scale structures (means and stresses), but it does not ensure a correct simultaneous simulation of small scale structures. The latter is only the case if the dynamic method is designed in consistency with a realizable stress model (as given for the LDM). This conclusion has relevant implications. It means that a dynamic LES method does not have predictive power in general (such that it can be used without evidence as an alternative to DNS to simulate moderate Reynolds number flows). On the other hand, the results reported here support the view that the LDM has such predictive power because large and small scale structures can be correctly represented simultaneously. Evidence for the conclusions will be presented in the talk by also including dynamic LES results of periodic hill flows at high Reynolds numbers.

REFERENCES

Coleman, G. N., Ferziger, J. H. & Spalart, P. R. 1990 A numerical study of the Ekman layer. *Journal of Fluid Mechanics* **213**, 313–248.

Germano, M. 1992 Turbulence- The filtering approach. *Journal of Fluid Mechanics* **238**, 325–336.

Germano, M., Piomelli, U., Moin, P. & Cabot, W.H. 1991 A dynamic subgrid-scale eddy viscosity model. *Physics of Fluids A: Fluid Dynamics* **3** (7), 1760–1765.

Gullbrand, J. & Chow, F. K. 2003 The effect of numerical errors and turbulence models in large-eddy simulations of channel flow, with and without explicit filtering. *Journal of Fluid Mechanics* **495**, 323–341.

Heinz, S. 2008 Realizability of dynamic subgrid-scale stress models via stochastic analysis. *Monte Carlo Methods and Applications* **14** (4), 311–329.

Heinz, S. & Gopalan, H. 2012 Realizable versus non-realizable dynamic subgrid-scale stress models. *Physics of Fluids* **24** (11), 115105/1–23.

Issa, R. I. 1986 Solution of the implicitly discretised fluid flow equations by operator-splitting. *Journal of computational physics* **62** (1), 40–65.

Kazemi, E. 2014 Direct and large eddy simulation of the turbulent Ekman layer. In *PhD Thesis, Mathematics Department, University of Wyoming*.

Lilly, D. K. 1992 A proposed modification of the Germano subgrid-scale closure method. *Physics of Fluids A* **4** (3), 633–635.

Marlatt, W. 1994 Direct numerical simulation of Ekman layer transition and turbulence. PhD Thesis, University of Colorado, Boulder.

Moser, R. D., Kim, J. & Mansour, N. N. 1999 Direct numerical simulation of turbulent channel flow up to Re_τ= 590. *Physics of Fluids* **11** (4), 943–945.

Shingai, K. & Kawamura, H. 2002 Direct numerical simulation of turbulent heat transfer in the stably stratified Ekman layer. *Thermal Science and Engineering* **10** (1), 25–33.

Wang, B. C. & Bergstrom, D. J. 2005 A dynamic nonlinear subgrid-scale stress model. *Physics of Fluids* **17**, 035109/1 – 17.